JACS
JOURNAL OF THE AMERICAN CHEMICAL SOCIETY

Article

pubs.acs.org/JACS

Computational Studies on the Excited States of Luminescent Platinum(II) Alkynyl Systems of Tridentate Pincer Ligands in Radiative and Nonradiative Processes

Wai Han Lam,* Elizabeth Suk-Hang Lam, and Vivian Wing-Wah Yam*

Institute of Molecular Functional Materials and Department of Chemistry, The University of Hong Kong, Pokfulam Road, Pokfulam, Hong Kong, People's Republic of China

Supporting Information

ABSTRACT: Platinum(II) alkynyl complexes of various tridentate pincer ligands, $[Pt(trpy)(C{\equiv}CR)]^+$ (trpy = 2,2′:6′,2″-terpyridine), $[Pt(R'\text{-bzimpy})(C{\equiv}CR)]^+$ (R′-bzimpy = 2,6-bis(*N*-alkylbenzimidazol-2′-yl)pyridine and R′ = alkyl), $[Pt(R'\text{-bzimb})(C{\equiv}CR)]$ (R′-bzimb = 1,3-bis(*N*-alkylbenzimidazol-2′-yl)benzene and R′ = C_4H_9), have been found to possess rich photophysical properties. The emission in dilute solutions of $[Pt(trpy)(C{\equiv}CR)]^+$ originated from a triplet alkynyl-to-tridentate pincer ligand-to-ligand charge transfer (LLCT) excited state, with mixing of a platinum-to-tridentate pincer ligand metal-to-ligand charge transfer (MLCT) excited state, while that of $[Pt(R'\text{-bzimb})(C{\equiv}CR)]$ originated from a triplet excited state of intraligand (IL) character of the tridentate ligand mixed with a platinum-to-tridentate ligand MLCT character. Interestingly, both emissions were observed in $[Pt(R'\text{-bzimpy})(C{\equiv}CR)]^+$ in some cases. In addition, $[Pt(R'\text{-bzimb})(C{\equiv}CR)]$ displayed a photoluminescence quantum yield higher than that of $[Pt(R'\text{-bzimpy})(C{\equiv}CR)]^+$. Computational studies have been performed on the representative complexes $[Pt(trpy)(C{\equiv}CPh)]^+$ (**1**), $[Pt(R'\text{-bzimpy})(C{\equiv}CPh)]^+$ (**2**), and $[Pt(R'\text{-bzimb})(C{\equiv}CPh)]$ (**3**), where R′ = CH_3 and Ph = C_6H_5, to provide an in-depth understanding of the nature of their emissive origin as well as the radiative and nonradiative processes. In particular, the factors governing the ordering of the triplet excited states and radiative decay rate constants of the emissive state (^{3}ES) have been examined. The potential energy profiles for the deactivation process from the ^{3}ES via triplet metal-centered (^{3}MC) states have also been explored. This work reveals for the first time the potential energy profiles for the thermal deactivation pathway of square planar platinum(II) complexes.

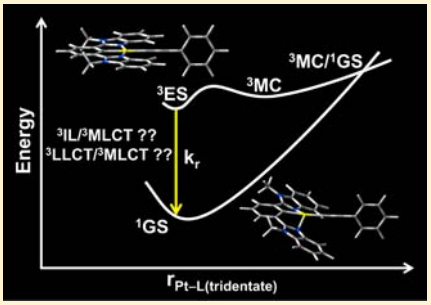

INTRODUCTION

Platinum(II) complexes with tridentate ligands have been extensively explored due to their rich spectroscopic properties and their wide range of applications from biological probes to optoelectronic devices.[1−5] A platinum(II) terpyridine alkynyl system, $[Pt(trpy)(C{\equiv}CR)]^+$, that exhibits long-lived emission in solution was reported by Yam and co-workers.[2] The emission was assigned as originating from the triplet ligand-to-ligand charge transfer (^{3}LLCT) from the alkynyl to terpyridine mixed with the platinum-to-terpyridine metal-to-ligand charge transfer (^{3}MLCT) excited state.[2a] Since the emission color of $[Pt(trpy)(C{\equiv}CR)]^+$ can be tuned upon incorporation of different functionalized alkynyl ligands, they have been employed for various applications such as in pH and cation sensing.[2c−f]

In addition to platinum(II) terpyridine complexes, another class of platinum(II) N^N^N system, with 2,6-bis(*N*-alkylbenzimidazol-2′-yl)pyridine (R′-bzimpy, where R′ = alkyl) has been investigated.[3] Similar to the platinum(II) terpyridine system, the photoluminescence quantum yields of these platinum(II) bzimpy alkynyl complexes in CH_2Cl_2 are on the order of 10^{-2}.[2b,3a] In addition, the emission for $[Pt(R'\text{-bzimpy})(C{\equiv}CR)]^+$, where R′ = $C_{12}H_{25}$, originated from the ^{3}LLCT/^{3}MLCT [$\pi(C{\equiv}CR)/d\pi(Pt) \rightarrow \pi^*(bzimpy)$] excited state,[3a] while with the alkynyl ligands (R = C_6H_5, C_6H_4Me), both triplet intraligand (^{3}IL)/^{3}MLCT [$\pi(bzimpy)/d\pi(Pt) \rightarrow \pi^*(bzimpy)$] and ^{3}LLCT/^{3}MLCT emissions were observed in solution at room temperature,[3a] demonstrating that the emissive origin in solution of $[Pt(R'\text{-bzimpy})(C{\equiv}CR)]^+$ is sensitive toward both the solvent and the *para* substituents on the arylalkynyl ligands employed.[3a] A fine perturbation of the electron-richness of the alkynyl ligand or a change in the solvent polarity has been shown to switch the emission properties from a ^{3}LLCT/^{3}MLCT origin to a ^{3}IL origin and vice versa.[3a] Moreover, with the incorporation of hydrophobic and solubilizing groups, organogelation was observed.[3b] Luminescence enhancement upon a gel-to-sol phase transition[3b] and formation of self-assembled nanostructures with interesting morphological transformation from vesicles to nanofibers have been demonstrated.[3c]

Upon changing the central pyridine ring of the bzimpy system to the benzene ring of the cyclometalated 1,3-bis(*N*-alkylbenzimidazol-2′-yl)benzene (R′-bzimb, where R′ = C_4H_9) ligand system, the photophysical behaviors are dramatically changed. In contrast to the platinum(II) bzimpy system with

Received: July 4, 2013
Published: September 26, 2013

   dx.doi.org/10.1021/ja406810a | *J. Am. Chem. Soc.* 2013, 135, 15135−15143

Chart 1. Chemical Structures of 1−3

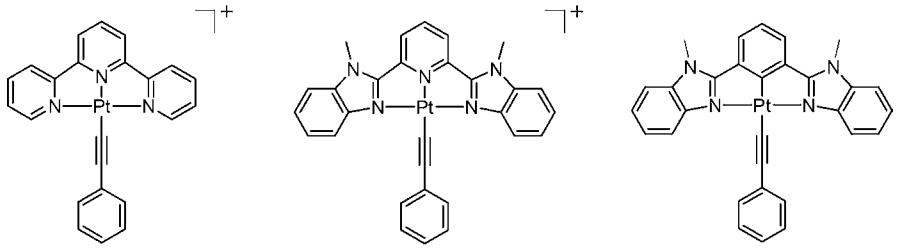

1 2 3

photoluminescence quantum yields of up to 10^{-2} only, upon incorporation of bzimb into platinum(II), a photoluminescence quantum yield as high as 0.67 was obtained.[4] The high photoluminescence quantum yield and the charge-neutral nature of the complexes have allowed these complexes to be utilized in the fabrication of phosphorescent organic light-emitting diodes (PHOLEDs) with good performance. Due to the ^{3}IL/^{3}MLCT nature of the emissive state, the emission color can be tuned by modification of different substituent groups at the 5-position of the aryl ring of the bzimb ligand.[4b]

It can be clearly seen that these three types of platinum(II) systems with tridentate pincer ligands possess quite different luminescence behaviors. It is unclear why emissions from both ^{3}LLCT/^{3}MLCT and ^{3}IL/^{3}MLCT excited states were observed for [Pt(R′-bzimpy)(C≡CR)]$^+$ complexes with particular alkynyl ligands, yet only one type of emission was observed in the [Pt(trpy)(C≡CR)]$^+$ and [Pt(R′-bzimb)(C≡CR)] complexes. To gain a better understanding of their luminescence behavior, it is essential to investigate the electronic structures and the factors that cause the changes in the relative energies of the low-lying excited states of the complexes.

Most platinum(II) R′-bzimb complexes have a photoluminescence quantum yield an order of magnitude higher than that of the R′-bzimpy counterparts. The photoluminescence quantum yield is determined by both the radiative and the nonradiative decay rate constants. In general, the radiative decay rate constant depends on the efficiency of spin−orbit coupling (SOC), which is enhanced by the presence of a heavy metal center such as platinum. Spin−orbit coupling mixes the singlet and triplet states via facile intersystem crossing (ISC), enabling the formally spin-forbidden singlet−triplet transitions to become allowed. This "allowedness" can also be related to the transition dipole moments of the transitions from the singlet ground state (^{1}GS) and the interacting singlet excited states. The energy gap between the interacting triplet and singlet excited states is also found to be one of the important factors which controls the radiative decay rate constant of the emissive state (ES).[5] However, it is unclear which factors would contribute most to the radiative decay rate constants of the platinum(II) systems mentioned above.

Other than the importance of the intrinsic radiative decay rate constants of the emissive state, the roles of metal-centered (MC) ligand field excited states are also very crucial in determining the photoluminescence efficiency of the transition metal complex systems.[6] For example, [Pt(trpy)(L)]$^{n+}$ (L = Cl, Br, I, N_3, or SCN, n = 1; L = NH_3, n = 2) complexes have been demonstrated to be emissive in the solid state and in low-temperature glass but not in room temperature solutions.[7a,b] This phenomenon can be ascribed to the thermal population of the MC state of d−d character.[7] Since the MC state involves population of the metal−ligand antibonding orbitals (dσ*), which would lead to a significant molecular distortion, it provides the effective paths for the radiationless decay and is responsible for the photochemical ligand labilization process.

Strategies to avoid the thermal population of the ^{3}MC states by "pushing" them to higher energies and making them thermally inaccessible at ambient temperature have been developed.[8] However, the information on the relative stabilities of the emissive and metal-centered states is rather limited for a more in-depth understanding of the deactivation process. In addition to the relative energies of the two states, the relative positions of the ^{3}MC/^{1}GS crossing point and the ^{3}ES−^{3}MC transition state are the key parameters for the nonradiative decay process. Several computational studies have been performed for the octahedral ruthenium(II) and iridium(III) complexes to investigate the reaction energy profile for the ^{3}MLCT−^{3}MC conversion.[9] However, to the best of our knowledge, there are no reports on the study of the potential energy profile for the deactivation pathway via the ^{3}MC state for the square planar d^8 platinum(II) complexes.

Herein are described the computational studies to investigate the electronic structures and the intrinsic radiative decay and nonradiative decay processes for the three platinum(II) tridentate pincer phenylalkynyl complexes, namely, [Pt(trpy)(C≡CPh)]$^+$ (**1**), [Pt(R′-bzimpy)(C≡CPh)]$^+$ (**2**), and [Pt(R′-bzimb)(C≡CPh)] (**3**), where the alkyl chains R′ are replaced by methyl groups, to understand the differences in their photoluminescence behavior in dilute solutions (Chart 1). In particular, the factors that determine the ordering of the triplet excited states and radiative decay rate constants of the emissive states have been examined. The potential energy profiles for the nonradiative deactivation process via the ^{3}MC states have also been explored. This study would hopefully provide crucial information for the future design of luminescent platinum(II) complexes, especially with the wide applications of platinum(II) complexes in optoelectronic devices and biological probes.

■ COMPUTATIONAL DETAILS

All the density functional theory (DFT) and time-dependent density functional theory (TDDFT) calculations were carried out by using Gaussian 09 software.[10] Geometry optimizations were performed for the ground states and triplet excited states of **1**−**3** as well as the transition states for the ^{3}ES−^{3}MC conversions in CH_2Cl_2 using density functional theory with the hybrid Perdew, Burke, and Ernzerhof functional (PBE0)[11] in conjunction with the conductor-like polarizable continuum model (CPCM).[12] The unrestricted formalism was used for the geometry optimization of triplet states. Vibrational frequencies were calculated for all stationary points to verify that each was a minimum (NIMAG = 0) or a transition state

dx.doi.org/10.1021/ja406810a | J. Am. Chem. Soc. 2013, 135, 15135−15143

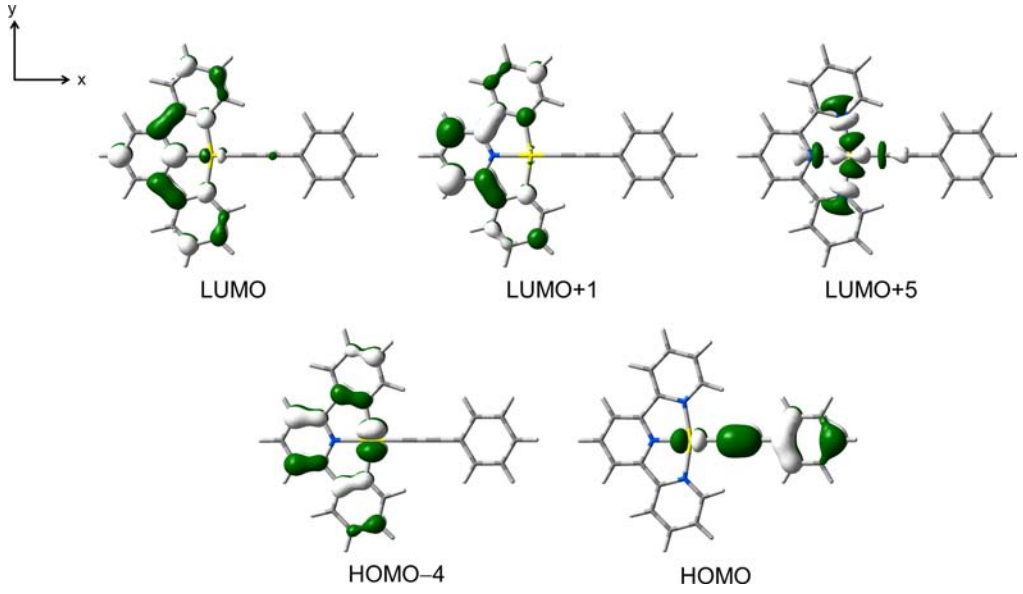

Figure 1. Spatial plots (isovalue 0.045) of selected molecular orbitals for **1** at the ground-state optimized geometry.

(NIMAG = 1) on the potential energy surface. Intrinsic reaction coordinate (IRC) calculations were also carried out to confirm the transition states connecting two relevant minima.[13] The minimum energy crossing points (MECPs) between the relevant potential energy surfaces were optimized using Gaussian 09 together with the code developed by Harvey et al.[14] On the basis of the optimized structures of the ground state and the triplet emissive state, TDDFT calculations[15] at the same level associated with the CPCM (CH_2Cl_2) were employed to compute singlet−singlet and singlet−triplet transitions for the study of the nature of emissive states and radiative decay rate constant, respectively. For all the calculations, the Stuttgart effective core potentials (ECPs) and the associated basis set were applied to describe Pt[16] with f-type polarization functions (ζ = 0.993),[17] whereas, for all other atoms, the 6-31G(d,p) basis set[18] was used. The squares of the Pt d orbital coefficients were obtained from c^2 in natural bond orbital (NBO) analysis[19] calculations and extracted using QMForge.[20]

Formalism for the Radiative Decay Rate Constant. The radiative decay rate constant (k_r^{α}) from substate α of the m^{th} triplet emissive states (T_m) for **1**−**3** can be expressed with the formalism[5]

$$k_r^{\alpha}(T_m \rightarrow S_0) = \frac{64\pi^4}{3h} E(T_m)^3 \left\{ \sum_{S_n} \frac{\langle T_m^{\alpha}|H_{SOC}|S_n\rangle}{E(S_n) - E(T_m)} \langle S_n|M|S_0\rangle \right\}^2 \quad (1)$$

where h is the Planck constant, H_{SOC} is the Hamiltonian of spin−orbit coupling, $E(T_m)$ and $E(S_n)$ are the unperturbed energies of the m^{th} triplet and n^{th} singlet excited states, respectively, and $\langle S_n|M|S_0\rangle$ is the transition dipole moment between the electronic ground state and n^{th} excited singlet state (S_n).

The evaluation of the spin−orbit coupling element $\langle H_{SOC}\rangle$ is given in the Supporting Information. The transition dipole moment is related to the oscillator strength by

$$\langle S_n|M|S_0\rangle^2 = \frac{3he^2}{8\pi m_e c} \frac{f_n}{E(S_n)} \quad (2)$$

where e is the electron charge, m_e is the mass of an electron, c is the speed of light, and f_n is the oscillator strength of S_n.[5d,e]

Equation 1 thus becomes

$$k_r^{\alpha}(T_m \rightarrow S_0) = \frac{8\pi^3 e^2}{m_e c} \left\{ \sum_n \frac{\langle T_1^{\alpha}|H_{SOC}|S_n\rangle}{\left(\frac{E(S_n)}{E(T_m)}\right)^{1/2}\left(\frac{E(S_n)}{E(T_m)} - 1\right)} f_n^{1/2} \right\}^2 \quad (3)$$

In the high-temperature limit, the triplet substates are assumed to be equally populated due to fast spin relaxation.[5f] Therefore, the radiative decay rate constant of the triplet emissive state is determined by the average of the k_r^{α} values:

$$k_r = \frac{1}{3} \sum k_r^{\alpha} \quad (4)$$

RESULTS AND DISCUSSION

Ordering of the Triplet Excited States. TDDFT/CPCM calculations have been performed for **1**−**3** at the ground-state optimized geometries to study the ordering of the triplet excited state to provide an understanding of the nature of their emissive states. Selected molecular orbitals for **1**−**3** are shown in Figure 1 and Supporting Information Figures S1 and S2. The highest occupied molecular orbital (HOMO) in each complex is the π orbital of the arylalkynyl ligand mixed with the platinum dπ orbital, while the lowest unoccupied molecular orbital (LUMO) is the π^* orbital of the tridentate ligand.

Selected singlet−triplet transitions for **1**−**3** are listed in Table 1. The lowest energy triplet excited state (T_1) of **1** and **2** arises from HOMO → LUMO excitation and consists of ^{3}LLCT/^{3}MLCT character. In contrast to **1** and **2**, the T_1 state of **3** has a ^{3}IL/^{3}MLCT character. It arises from HOMO−2 → LUMO excitation, where HOMO−2 is the highest energy π orbital of the bzimb ligand mixed with the metal dπ orbital.[4c] According to Kasha's rule, the emitting level of a given spin multiplicity is the lowest excited level of that spin multiplicity.[21] The computed results are consistent with the assignment of the emission for the three classes of complexes in the previous studies.[2a,3a,4b]

It is noted that the energy separations of the corresponding ^{3}IL/^{3}MLCT states in **1** and ^{3}LLCT/^{3}MLCT states in **3** from their corresponding T_1 states are large. The two lowest energy ^{3}LLCT/^{3}MLCT excited states for **3**, T_6(HOMO → LUMO)

dx.doi.org/10.1021/ja406810a | J. Am. Chem. Soc. 2013, 135, 15135−15143

Table 1. Selected Triplet Excited States (T_n) of 1−3 Computed by TDDFT/CPCM (CH_2Cl_2) at the Optimized Ground-State Geometries

complex	T_n	excitation[a]	coefficient[b]	vertical excitation energy (eV)	character[c]
1	T_1	H → L	0.67	2.08	^{3}LLCT/^{3}MLCT
	T_3	H−4 → L+1	0.52	2.81	^{3}IL/^{3}MLCT
	T_4	H−4 → L	0.63	2.87	^{3}IL/^{3}MLCT
	T_{14}	H → L+5	0.64	3.78	^{3}MC
2	T_1	H → L	0.65	2.16	^{3}LLCT/^{3}MLCT
	T_2	H−1 → L	0.66	2.36	^{3}IL/^{3}MLCT
	T_{18}	H → L+4	0.63	3.91	^{3}MC
3	T_1	H−2 → L	0.56	2.58	^{3}IL/^{3}MLCT
	T_6	H → L	0.70	3.24	^{3}LLCT/^{3}MLCT
	T_7	H → L+1	0.69	3.37	^{3}LLCT/^{3}MLCT
	T_{20}	H−2 → L+9	0.53	4.35	^{3}MC

[a]Orbitals involved in the major excitation (H = HOMO and L = LUMO). [b]Coefficients in the configuration interaction (CI) expansion. [c]Character of the excited state.

and T_7(HOMO → LUMO+1), are 0.66−0.79 eV higher in energy than the T_1 state. On the other hand, the two lowest energy ^{3}IL/^{3}MLCT excited states for **1**, T_3(HOMO−4 → LUMO+1) and T_4(HOMO−4 → LUMO), are 0.73−0.79 eV higher in energy than the T_1 state. This large energy separation between ^{3}IL/^{3}MLCT and ^{3}LLCT/^{3}MLCT excited states in the respective **1** and **3** are in line with the experimental observations, in which ^{3}IL/^{3}MLCT and ^{3}LLCT/^{3}MLCT emissions were not observed in the [Pt(trpy)(C≡CR)]$^+$ and [Pt(R′-bzimb)(C≡CR)] classes of complexes, respectively. As for complex **2**, the corresponding ^{3}IL/^{3}MLCT (T_2) state is only 0.20 eV higher in energy than the T_1 state. The relatively small energy difference of the two states might explain why emissions from both excited states were observed in some cases in the [Pt(bzimpy)(C≡CR)]$^+$ class of complexes.

To gain a better understanding of the ordering of triplet excited states in **1**−**3**, it is important to examine the electronic energy difference between the singlet and the triplet states. Triplet excited states are lower in energy than the singlet excited states with the same configuration due to a greater electron repulsion in the latter case. The singlet−triplet energy splitting (ΔE_{ST}) of the excited states with the same configuration is a result of the electron exchange integral, which is proportional to the spatial overlap of the orbitals involved in the electronic transition leading to the excited state. The ΔE_{ST} is small if the orbitals have a small spatial overlap. Therefore, it is expected that the ΔE_{ST} of the LLCT/MLCT states is generally smaller than that of the IL/MLCT states.

Selected singlet−singlet transitions are listed in Tables S1−S3 of the Supporting Information. One can see that the S_1 state corresponds to the ^{1}LLCT/^{1}MLCT state (HOMO → LUMO) for **1**−**3**, yet unlike **1** and **2** where T_1 is the ^{3}LLCT/^{3}MLCT state with the same configuration, the T_1 state in **3** is the ^{3}IL/^{3}MLCT state. The ^{1}LLCT/^{1}MLCT state in **3** is computed to be slightly lower in energy than the ^{1}IL/^{1}LLCT state (0.28 eV). On the other hand, the ΔE_{ST} of the IL/MLCT states (0.95 eV) is significantly larger than that of the LLCT/MLCT states (0.01 eV) due to a large spatial overlap of the π and π^* orbitals of the bzimb ligand. The larger ΔE_{ST} of the IL/MLCT states would compensate for the inherent energy difference between the ^{1}IL/^{1}MLCT and ^{1}LLCT/^{1}MLCT states, leading to a change in the character of the S_1 and T_1 states.

When compared to **3**, a larger energy separation between the ^{1}LLCT/^{1}MLCT and ^{1}IL/^{1}MLCT states (1.01 eV) is found in **1** due to a less extended π-conjugation of the terpyridine ligand, leading to a higher-lying ^{1}IL/^{1}MLCT state. The large energy separation between the ^{1}LLCT/^{1}MLCT state and the ^{1}IL/^{1}MLCT state could outweigh the ΔE_{ST} of the IL/MLCT states, rendering the ^{3}LLCT/^{3}MLCT state as the T_1 state.

Similar to **3**, the ^{1}IL/^{1}MLCT state in **2** is also only slightly higher in energy than the ^{1}LLCT/^{1}MLCT state (0.36 eV). However, it is interesting to note that the difference in the ΔE_{ST} of the IL/MLCT states (0.39 eV) and LLCT/MLCT states (0.23 eV) is much smaller than that in **3**. A closer look at the molecular orbitals involved in the IL/MLCT transition in **2** reveals that the π orbital is more localized on the benzimidazole rings, while the π^* orbital is localized on the central pyridine ring. The smaller spatial overlap of the two orbitals reduces the ΔE_{ST} of the IL/MLCT states, resulting in a smaller energy gap between the ^{3}IL/^{3}MLCT and ^{3}LLCT/^{3}MLCT states.

Photoluminescence Quantum Yield. Experiments have shown that the photoluminescence quantum yield increases dramatically upon changing the ligand from bzimpy to bzimb. For example, [Pt(R′-bzimpy)(C≡CR)]$^+$ complexes were shown to display rather low photoluminescence quantum yield in solution ranging from less than 0.01 to 0.096,[3a] while [Pt(bzimb)(C≡CR)] complexes, obtained by switching the central pyridine ring to a benzene ring, can exhibit a photoluminescence quantum yield as high as 0.67.[4c] The terpyridine complexes of the N^N^N-type ligand exhibit photoluminescence quantum yields similar to that of bzimpy. The photoluminescence quantum yield is determined by the radiative and nonradiative decay rate constants. In the following section, the factors which determine the radiative decay rate constant will be discussed.

Radiative Decay Rate Constant. To elucidate the radiative decay rate constant (k_r) of **1**−**3**, computational analysis based on eq 3 has been performed for the optimized structures of the emissive states of **1**−**3**. A plot of the spin density of the ^{3}LLCT/^{3}MLCT excited states of **1** and **2** and the ^{3}IL/^{3}MLCT excited state of **3** is shown in Figure S3 (Supporting Information). Tables S4−S7 of the Supporting Information list the selected singlet−singlet and singlet−triplet transitions of **1**−**3** for the evaluation of the radiative decay rate constants. In this study, the first 10 singlet excited states are considered in the spin−orbit coupling formalism. The calculated radiative decay rate constants of **1**−**3** are shown in Table 2.

dx.doi.org/10.1021/ja406810a | J. Am. Chem. Soc. 2013, 135, 15135−15143

Table 2. Calculated Radiative Decay Rate Constants for Complexes 1−3

complex	emissive state	k_r (s^{-1})
1	^{3}LLCT/^{3}MLCT	6.09×10^3
2	^{3}LLCT/^{3}MLCT	6.73×10^4
3	^{3}IL/^{3}MLCT	8.69×10^4

According to eq 3, there are three factors governing the radiative rate constant. They are the strength of the spin−orbit coupling interaction $\langle S_n|H_{SOC}|T_1\rangle$ between the higher-lying singlet excited states (S_n) and the ^{3}ES, the oscillator strength (f) of the S_n states which can couple with the ^{3}ES, and the energy separation between the coupled states.

The strength of the spin−orbit coupling interaction depends on the spin−orbit coupling element of higher-lying S_n and the ^{3}ES. The spin−orbit operator of many-electron states is treated as a sum of one-particle operators. As the spin−orbit coupling constant (ξ = 4626 cm^{-1})[22] for platinum is larger than that of other atoms in **1**−**3**, spin−orbit coupling involving atoms other than platinum is neglected. Therefore, an increase in the platinum d contribution in the molecular orbitals associated with the ^{3}ES would enhance spin−orbit coupling. Under the spin−orbit formalism, the electronic configuration $^3[(d)^1(\pi^*)^1]$ in the ^{3}ES can only effectively couple with those S_n states having specific $^1[(d)^1(\pi^*)^1]$ configurations involving different d orbitals and a common π^* orbital.[5a]

Figure 2 shows the singlet excited states that can couple with the ^{3}ES. As depicted in Figure 2, **1** has the least available singlet excited states (S_3, S_4, S_5, and S_7). Among the four singlet excited states, the S_7 state cannot effectively couple with the ^{3}ES, as there is no platinum d orbital contribution in the configuration ascribed to the S_7 state (first value in parentheses in Figure 2). Tables S8−S10 of the Supporting Information list the c coefficients of the platinum d orbitals in selected occupied molecular orbitals of **1**−**3**. It is also noted that the oscillator strength (f, second value in parentheses in Figure 2) is zero for the $S_0 \rightarrow S_3$ transition, indicating the transition is forbidden. With reference to eq 3, the feasibility of transitions from the ground state to the interacting singlet states also plays a crucial role in determining the radiative rate constant. Therefore, the coupling between the S_3 state and the ^{3}ES is not effective. Although the ^{3}ES's of both **1** and **2** are the ^{3}LLCT/^{3}MLCT states, **2** has more singlet excited states which can couple with ^{3}ES than **1**. As a result, **2** has a larger radiative decay rate constant than **1**.

For **2** and **3**, although the energy gap for those singlet excited states that can couple with the ^{3}ES are similar, it is found that the contribution of the d orbitals to the electronic configurations ascribed to the ^{3}ES of **3** is larger than that for **2**. Considering the same ^{1}MLCT states in **2** (S_5) and **3** (S_6) corresponding to the excitation from the metal d_{z^2} orbital to the LUMO, the ^{3}ES in **3** has a larger spin−orbit coupling element than that in **2**. This shows that a larger platinum d orbital participation in the ^{3}ES of **3** (^{3}IL/^{3}MLCT) than that of **2** (^{3}LLCT/^{3}MLCT) is one of the reasons for the larger k_r in **3** than in **2**.[23] In addition, most of the available S_n states of **2** have smaller oscillator strengths than those of **3** from where the ^{3}ES can borrow its intensity. The only exception is the S_7 state in **2**, yet the platinum d orbital participation is relatively small, which leads to a smaller k_r for **2** than for **3**.

Nonradiative Decay Process. Thermal population to the ^{3}MC state from the ^{3}ES is an effective pathway for nonradiative decay. Therefore, the accessibility of this ^{3}MC state can be expected to have profound effects on the luminescence properties of the metal complexes. Among **1**−**3**, one would expect that **3** has a higher energy ^{3}MC state because of the presence of a strong-field C donor relative to that of the N donor. Nevertheless, the situation is complicated since **3** also has a higher energy ES. For a more detailed picture of the excited-state processes, which is crucial to the understanding of the phosphorescent behavior of this class of materials, knowledge of the potential energy profiles of the deactivation pathway from the ^{3}ES via the ^{3}MC state in **1**−**3** is necessary.

The MC state for the d^8 square planar complexes is formed by population of the $d\sigma^*$ orbital, which is comprised of the metal $d_{x^2-y^2}$ orbital and ligand σ orbitals. From the TDDFT/CPCM calculations at the ground-state optimized geometry of **1**−**3**, the lowest energy ^{3}MC transition corresponds to the excitation from the HOMO [$d\pi$(Pt)−π(C≡CR) orbital] to

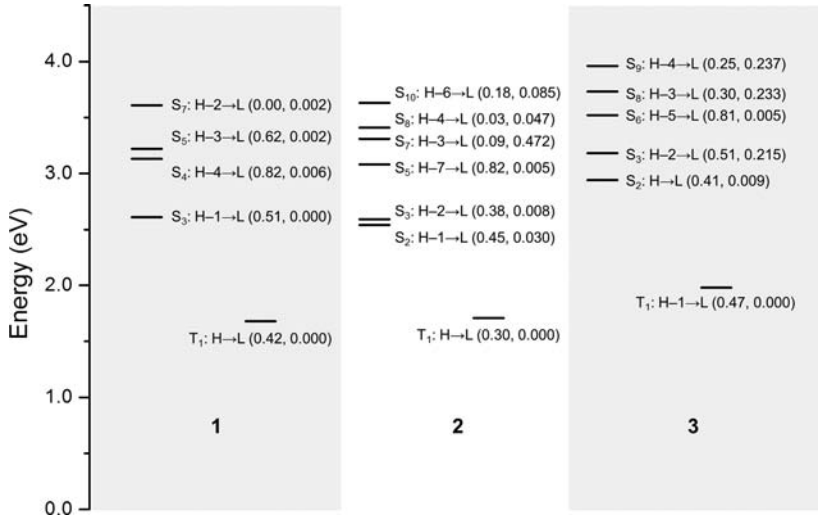

Figure 2. Energy level diagrams of selected excited states with their major excitation in **1**−**3**. Only the S_n states that can couple with T_1 (^{3}ES) are shown. The first and second values in parentheses are the largest c coefficient of d orbitals involved in the excitation and the oscillator strength of the transitions, respectively.

dx.doi.org/10.1021/ja406810a | J. Am. Chem. Soc. 2013, 135, 15135−15143

the dσ* orbital for **1** (T_{14} state) and **2** (T_{18} state). However, the lowest energy ^{3}MC state for **3** corresponds to the excitation from the HOMO−2 (dπ(Pt)−π(N^C^N) orbital) to the dσ* orbital (T_{20} state). The relative energies of the ^{3}MC state to the ^{3}ES are similar (1.70, 1.75, and 1.77 eV for **1**, **2**, and **3**, respectively), even though **3** has a higher-lying ^{3}MC state (Table 1).

On the basis of the major excitation in the lowest energy ^{3}MC state obtained from TDDFT calculations, geometry optimizations of the lowest energy ^{3}MC state for **1**−**3** have been performed. Figure 3 shows the singly occupied molecular orbitals (SOMOs) of the optimized structures of the ^{3}MC states for **1**−**3**. The higher energy SOMO in each complex is similar to the dσ* orbital in the ground-state optimized geometry (Figure 1 and Supporting Information Figures S1 and S2). The lower energy SOMO for **1** and **2** is the dπ(Pt)−π(C≡CPh) antibonding orbital. Different from those of **1** and **2**, the dπ orbital of **3** is almost perpendicular to the Pt(N^C^N) molecular plane. In addition, less contribution of the alkynyl ligand is found in the two SOMOs for **3**, when compared with **1** and **2**. Figure 4 depicts a plot of the spin density for the ^{3}MC states. The Mulliken atomic spin density at the platinum center is 1.07, 1.08, and 1.43 for **1**, **2**, and **3**, respectively, which is significantly larger than that for the corresponding ^{3}ES.

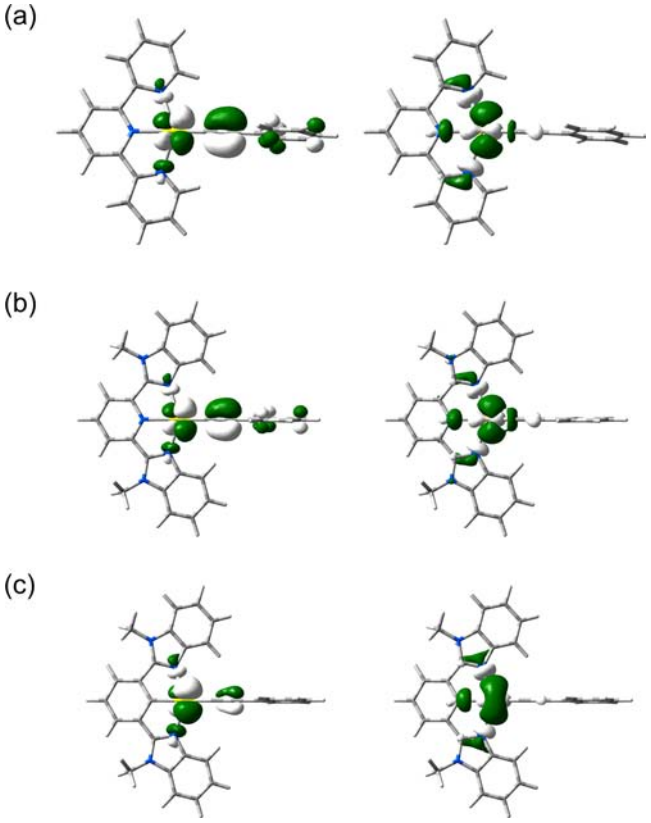

Figure 3. Spatial plot (isovalue 0.045) of the lower energy (left) and higher energy (right) SOMOs for **1** (a), **2** (b), and **3** (c) at the optimized structures of the ^{3}MC state obtained from restricted open-shell (RO)-PBE0 calculation.

The structural distortion energies of the ^{3}ES and ^{3}MC states in **1**−**3**, which are calculated as the difference between the ground-state energies at the corresponding ground-state and excited-state equilibrium geometries, are in the range of 4.6−8.5 and 32.5−36.7 kcal mol^{-1}, respectively, indicating that the ^{3}MC states exhibit more significant structural distortion than that for the emissive states. Tables S11−S13 of the Supporting Information list the selected structural parameters of the ^{3}MC states for **1**−**3**, and Figure S4 (Supporting Information) shows the optimized geometry of the ^{3}MC states. The structures of the ^{3}MC states are nonplanar, in which the average interplanar angles between the central ring and the two peripheral rings of the tridentate ligand, which is a measure of the planarity of the tridentate ligands, are in the range of 11.5°, 16.7°, and 20.0° for **1**, **2**, and **3**, respectively. The distortion is illustrated in Chart 2. The two peripheral pyridines of the tridentate ligand are bending down, while the central pyridine and alkynyl units are slightly bending up.

For **1** and **2**, all the Pt−N bond distances of the tridentate ligand in the ^{3}MC states are significantly increased by 0.189−0.232 and 0.178−0.198 Å relative to their corresponding ground states. On the other hand, the change in the Pt−C(alkynyl) bond distance is less significant, in which a shortening of 0.066 Å for **1** and 0.053 Å for **2** was observed. In general, the population of the dσ* orbital should result in M−L bond weakening. However, since electron density is removed from the dπ(Pt)−π(C≡CPh) antibonding orbital, a shortening of the Pt−C(alkynyl) bond is observed instead. The N(1)−Pt−N(3) and N(2)−Pt−C(1) bond angles in **1** and **2** are decreased from 159.1−161.1° and 180.0° to 136.1−138.6° and 170.4−171.0°, respectively. A similar distortion is found in the ^{3}MC state of **3** compared to **2**. It is worth mentioning that the elongation of the Pt−N(benzimidazole) bond distances of the tridentate ligand in the ^{3}MC state of **3** (0.250 Å) is more significant than that in **2** (0.178−0.184 Å).

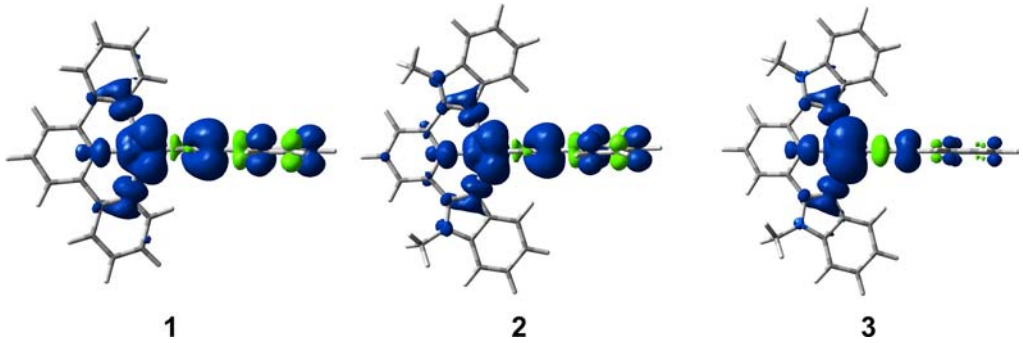

Figure 4. Spin density (isovalue 0.002) of the ^{3}MC states for **1**−**3**.

dx.doi.org/10.1021/ja406810a | J. Am. Chem. Soc. 2013, 135, 15135−15143

Chart 2. Diagram Showing the Excited-State Distortion

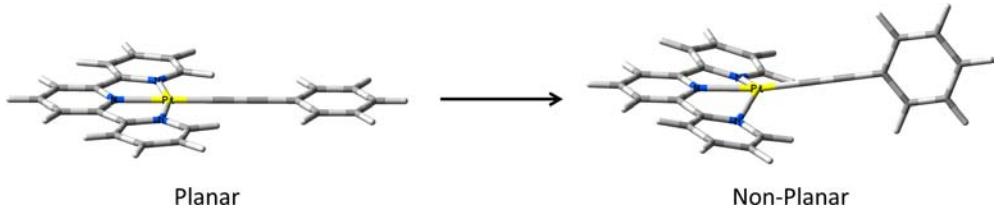

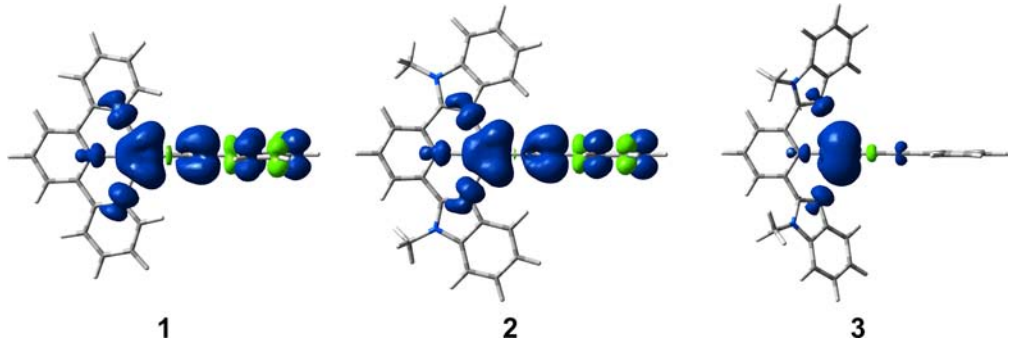

Figure 5. Spin density (isovalue 0.002) of the ^{3}MC/^{1}GS crossing points for **1**−**3**.

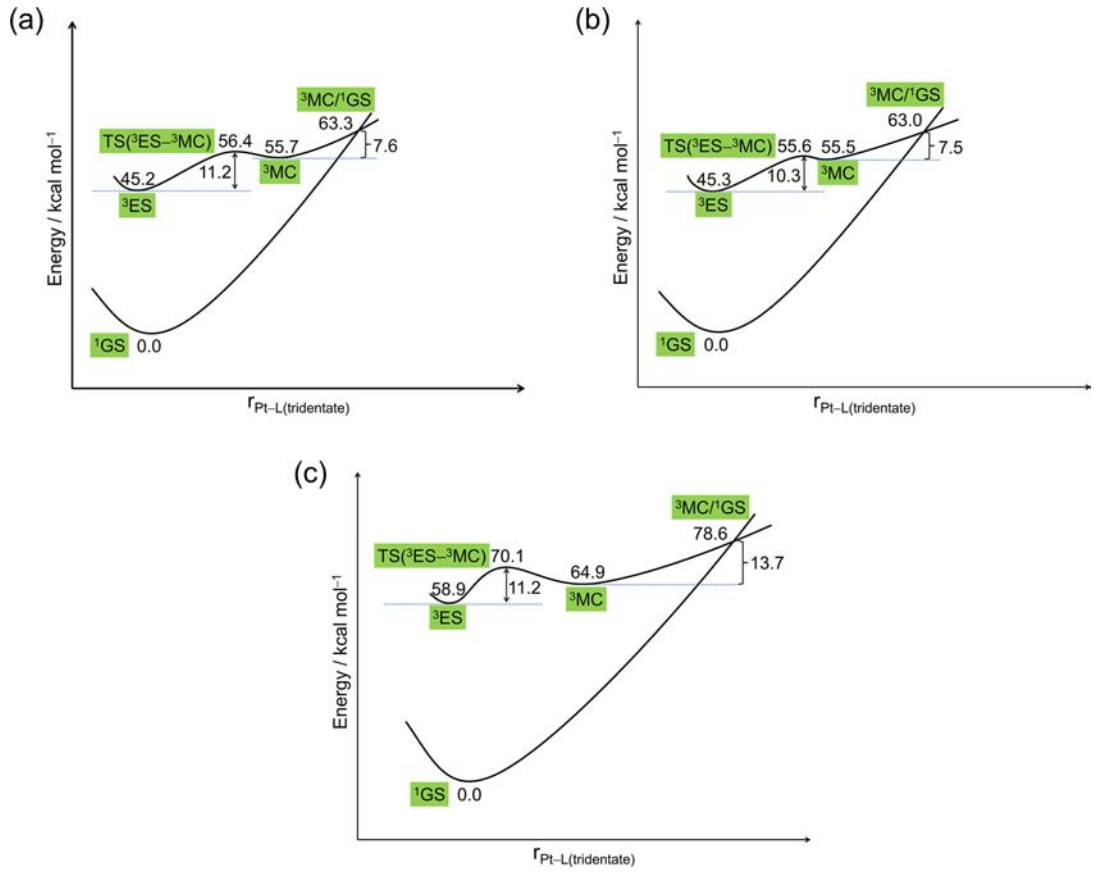

Figure 6. Schematic potential energy profiles of the deactivation pathway via the ^{3}MC state for **1** (a), **2** (b), and **3** (c).

The ^{3}MC state for **1**−**3** is 55.7, 55.5, and 64.9 kcal mol^{-1} higher in energy than the corresponding ground states. Introduction of the strong-field C donor in **3** indeed raises the energy of the ^{3}MC state. However, due to the higher energy of the emissive state in **3**, the relative energy of the ^{3}MC state to the ^{3}ES is only 6.0 kcal mol^{-1}, which is smaller than that in **1** (10.5 kcal mol^{-1}) and **2** (10.2 kcal mol^{-1}).

The transition states [TS(^{3}ES−^{3}MC)] connecting the two states for the ^{3}ES → ^{3}MC conversion have been determined. The higher energy SOMO shows a mixing of the π^* orbital of the tridentate ligand in the dσ^* orbital. Figure S5 of the Supporting Information depicts a plot of the spin density for the transition states. Similar to the structures of the ^{3}MC states, the transition states are also nonplanar. As shown in Tables

dx.doi.org/10.1021/ja406810a | J. Am. Chem. Soc. 2013, 135, 15135−15143

S11−S13 (Supporting Information), the Pt−L bond distances (L = C or N) of the metal-pincer ligand moiety are increased along the ^{3}ES → ^{3}MC path. The activation barrier for the ^{3}ES → ^{3}MC conversion of **3** is 11.2 kcal mol^{-1}, which is almost comparable to that of **1** (11.2 kcal mol^{-1}) and **2** (10.3 kcal mol^{-1}), even though the relative energy difference of the two states is smaller in **3**.

Once the ^{3}MC state is populated, it can either return to the ^{3}ES or encounter the MECP between the ^{3}MC and the ^{1}GS potential surfaces. If the ^{3}MC/^{1}GS crossing region lies close in energy to the ^{3}MC state and provided that the system has enough energy to reach the ^{3}MC state, it is likely that it would undergo fast decay back to the ground state. To investigate the feasibility of the regeneration of the ^{1}GS from the ^{3}MC state, the MECPs between the ^{3}MC and ^{1}GS surfaces for **1**−**3** were optimized. The structures and the plots of spin density of the ^{3}MC/^{1}GS crossing points are shown in Figure S6 of the Supporting Information and Figure 5, respectively.

The details of the potential energy curves relevant to the deactivation pathway are shown in Figure 6. The schematic plots are constructed by using the electronic energy of the calculated stationary points [S_0, ^{3}ES, TS(^{3}ES−^{3}MC), ^{3}MC] and MECP along the nuclear distortion coordinate, which indicates the relative change of the Pt−L (C or N) bond distances of the tridendate ligand with respect to those in the ground state. The ^{3}MC/^{1}GS crossing point for **1** is found to be 7.6 kcal mol^{-1} above the minimum of the ^{3}MC state (Figure 6a). Comparison of the geometrical structure of the ^{3}MC state and the ^{3}MC/^{1}GS crossing point is given in Table S11 (Supporting Information). Along the ^{3}ES → ^{3}MC → ^{3}MC/^{1}GS relaxation pathway, one can see that the alkynyl ligand stays very close to the platinum atom, while all the Pt−N bond distances are further lengthened from the ^{3}MC state to the ^{3}MC/^{1}GS crossing point. The structure at the crossing point is relatively planar when compared to that of the ^{3}MC state, as shown by the decrease of the interplanar angles between the central ring and the two peripheral rings of the tridentate ligand. Similar structural changes are found in **2** and **1** along the ^{3}ES → ^{3}MC → ^{3}MC/^{1}GS relaxation pathway. The ^{3}MC/^{1}GS crossing point for **2** is found to be 7.5 kcal mol^{-1} above that of the ^{3}MC state. The potential energy profile for the deactivation process in **2** is similar to that of **1** (see Figure 6b).

The structure of the ^{3}MC/^{1}GS crossing point for **3** is significantly different from that of **1** and **2**. When compared to the ^{3}MC state, the structure for the ^{3}MC/^{1}GS crossing point becomes more nonplanar, in which interplanar angles between the central ring and two peripheral rings of the tridentate ligand are increased by 20.1−20.4°. The platinum is still bonded to the carbon atom of the tridentate ligand, while the other nitrogen atoms are detached from the platinum center with Pt−N separations of 2.952−2.958 Å (Figure S6, Supporting Information). This crossing point for **3** is computed to be 13.7 kcal mol^{-1} above the minimum of the ^{3}MC state (Figure 6c). Even though the activation barrier for ^{3}ES → ^{3}MC is similar for all the complexes, the higher energy required to gain access from the ^{3}MC state to the ^{3}MC/^{1}GS crossing point would render the deactivation process in **3** energetically less favorable when compared to that of **1** and **2**.

On the basis of the calculations, **2** has a higher radiative decay rate constant than **1**, but they show a similar energetic profile for the deactivation pathway. One would expect that **2** should have a higher photoluminescence quantum yield than **1**. However, the photoluminescence quantum yield of **2** is comparable to that of **1**. Presumably, the floppiness of the complexes with the presence of the long alkyl chains attached to the nitrogen atoms of the bzimpy ligand would undergo facile nonradiative decay, dissipating the energy of the emissive excited state. On the other hand, **3** has a higher radiative decay rate constant as well as a kinetically less accessible nonradiative deactivation pathway than **2**. These could favor a higher photoluminescence quantum yield in **3** than in **2**.

CONCLUSION

DFT and TDDFT calculations have been successfully performed to provide a more in-depth insight into the nature of the emissive states as well as the radiative and nonradiative decay processes of the three platinum(II) alkynyl complexes of tridentate pincer ligands. It is found that the energy separation between the ^{3}LLCT/^{3}MLCT and ^{3}IL/^{3}MLCT excited states is governed by the extent of π-conjugation of the tridentate ligand and the singlet−triplet energy splitting of each excited state. In addition, the factors which govern the radiative decay rate constants and the potential energy profiles of the deactivation pathway via the ^{3}MC states have been examined. The results show that the radiative decay rate constant of **3** is larger than that of **2** because of the larger metal character in the emissive states and a larger allowedness of the coupled singlet excited state. The smaller radiative decay rate constant of **1** compared to **2** is ascribed to the lack of singlet excited states which can be effectively coupled with the triplet emissive state. The deactivation process via the ^{3}MC state of **3** is energetically less feasible than that of **1** and **2** because of the higher energy required in gaining access to the ^{3}MC/^{1}GS crossing point. It is important to note that the information on the relative energies of the ^{3}ES and ^{3}MC states would not be the sole factor to determine the feasibility of the nonradiative process via the MC state.

ASSOCIATED CONTENT

Supporting Information

Formalism of spin−orbit coupling, selected singlet excited states of **1**−**3** at the ground-state optimized structures, selected singlet and triplet excited states at the optimized geometries of the triplet emissive state, *c* coefficients of platinum d orbitals in selected molecular orbitals, selected structural parameters of the singlet ground state, triplet excited states, and MECPs for **1**−**3**, selected molecular orbitals for **2** and **3**, plots of the spin density of the emissive states and transition states for **1**−**3**, optimized structures of the ^{3}MC states and ^{3}MC/^{1}GS crossing point of **1**−**3**, complete ref 7, and Cartesian coordinates of the structures reported in the paper and their calculated (U)PBE0 electronic energies (hartrees). This material is available free of charge via the Internet at http://pubs.acs.org

AUTHOR INFORMATION

Corresponding Authors

chsue@hku.hk
wwyam@hku.hk

Notes

The authors declare no competing financial interest.

ACKNOWLEDGMENTS

We acknowledge support from The University of Hong Kong under the URC Strategic Research Theme on New Materials.

This work has been supported by the University Grants Committee Areas of Excellence Scheme (Grant AoE/P-03/08). E.S.-H.L. acknowledges the receipt of a Postgraduate Studentship from The University of Hong Kong. We are grateful to the Information Technology Services of The University of Hong Kong for providing computational resources.

REFERENCES

(1) (a) Lippard, S. J. *Acc. Chem. Res.* **1978**, *11*, 211. (b) Jennette, K. W.; Lippard, S. J.; Vassiliades, G. A.; Bauer, W. R. *Proc. Natl. Acad. Sci. U.S.A.* **1974**, *71*, 3839. (c) Becker, K.; Herold-Mende, C.; Park, J. J.; Lowe, G.; Schirmer, R. H. *J. Med. Chem.* **2001**, *44*, 2784. (d) Ratilla, E. M. A.; Brothers, H. M., II; Kostic, N. M. *J. Am. Chem. Soc.* **1987**, *109*, 4592.

(2) (a) Yam, V. W.-W.; Tang, R. P.-L.; Wong, K. M.-C.; Cheung, K.-K. *Organometallics* **2001**, *20*, 4476. (b) Yang, Q.-Z.; Wu, L.-Z.; Wu, Z.-X.; Zhang, L.-P.; Tung, C.-H. *Inorg. Chem.* **2002**, *41*, 5653. (c) Wong, K. M.-C.; Tang, W.-S.; Lu, X.-X.; Zhu, N.; Yam, V. W.-W. *Inorg. Chem.* **2005**, *44*, 1492. (d) Lo, H.-S.; Yip, S.-K.; Wong, K. M.-C.; Zhu, N.; Yam, V. W.-W. *Organometallics* **2006**, *25*, 3537. (e) Wong, K. M.-C.; Yam, V. W.-W. *Coord. Chem. Rev.* **2007**, *251*, 2477. (f) Wong, K. M.-C.; Yam, V. W.-W. *Chem. Commun.* **2011**, *47*, 11579. (g) Leung, S. Y.-L.; Tam, A. Y.-Y.; Tao, C.-H.; Chow, H. S.; Yam, V. W.-W. *J. Am. Chem. Soc.* **2012**, *134*, 1047.

(3) (a) Tam, A. Y.-Y.; Lam, W. H.; Wong, K. M.-C.; Zhu, N.; Yam, V. W.-W. *Chem.—Eur. J.* **2008**, *14*, 4562. (b) Tam, A. Y.-Y.; Wong, K. M.-C.; Yam, V. W.-W. *J. Am. Chem. Soc.* **2009**, *131*, 6253. (c) Po, C.; Tam, A. Y.-Y.; Wong, K. M.-C.; Yam, V. W.-W. *J. Am. Chem. Soc.* **2011**, *133*, 12136.

(4) (a) Tam, A. Y.-Y.; Tsang, D. P.-K.; Chan, M.-Y.; Zhu, N.; Yam, V. W.-W. *Chem. Commun.* **2011**, *47*, 3383. (b) Lam, E. S.-H.; Tsang, D. P.-K.; Lam, W. H.; Tam, A. Y.-Y.; Chan, M.-Y.; Wong, W.-T; Yam, V. W.-W. *Chem.—Eur. J.* **2013**, *19*, 6385. (c) Lam, E. S.-H.; Tam, A. Y.-Y.; Lam, W. H.; Wong, K. M.-C.; Zhu, N.; Yam, V. W.-W. *Dalton Trans.* **2012**, *41*, 8773.

(5) (a) Yersin, H., Ed. *Highly Efficient OLEDs with Phosphorescent Materials*; Wiley-VCH: Weinheim, Germany, 2007. (b) Yersin, H.; Rausch, A. F.; Czerwieniec, R.; Hofbeck, T.; Fischer, T. *Coord. Chem. Rev.* **2011**, *255*, 2622. (c) Turro, N. J. *Modern Molecular Photochemistry*; Benjamin/Cummings Publishing: Menlo Park, NJ, 1978. (d) Tong, G. S.-M.; Che, C.-M. *Chem.—Eur. J.* **2009**, *15*, 7225. (e) Obara, S.; Itabashi, M.; Okuda, F.; Tamaki, S.; Tanabe, Y.; Ishii, Y.; Nozaki, K.; Haga, M. *Inorg. Chem.* **2006**, *45*, 8907. (f) Tatchen, J.; Waletzke, M.; Marian, C. M.; Grimme, S. *Chem. Phys.* **2001**, *264*, 245.

(6) (a) Wagenknechta, P. S.; Ford, P. C. *Coord. Chem. Rev.* **2011**, *255*, 591. (b) Islam, A.; Ikeda, N.; Nozaki, K.; Okamoto, Y.; Gholamkhass, B.; Yoshimura, A.; Ohno, T. *Coord. Chem. Rev.* **1998**, *171*, 355. (c) Williams, J. A. G. *Top. Curr. Chem.* **2007**, *281*, 205−268.

(7) (a) Yip, H.-K.; Cheng, L.-K.; Cheung, K.-K.; Che, C.-M. *J. Chem. Soc., Dalton Trans.* **1993**, 2933. (b) McMillin, D. R.; Moore, J. J. *Coord. Chem. Rev.* **2002**, *229*, 113. (c) Aldridge, T. K.; Stacy, E. M.; McMillin, D. R. *Inorg. Chem.* **1994**, *33*, 722.

(8) (a) Sajoto, T.; Djurovich, P. I.; Tamayo, A.; Yousufuddin, M.; Bau, R.; Thompson, M. E.; Holmes, R. J.; Forrest, S. R. *Inorg. Chem.* **2005**, *44*, 7992. (b) Haneder, S.; Da Como, E.; Feldmann, J.; Lupton, J. M.; Lennartz, C.; Erk, P.; Fuchs, E.; Molt, O.; Münster, I.; Schildknecht, C.; Wagenblast, G. *Adv. Mater.* **2008**, *20*, 3325. (c) Chang, C.-F.; Cheng, Y.-M.; Chi, Y.; Chiu, Y.-C.; Lin, C.-C.; Lee, G.-H.; Chou, P.-T.; Chen, C.-C.; Chang, C.-H.; Wu, C.-C. *Angew. Chem., Int. Ed.* **2008**, *47*, 4542. (d) Sajoto, T.; Djurovich, P. I.; Tamayo, A. B.; Oxgaard, J.; Goddard, W. A., III; Thompson, M. E. *J. Am. Chem. Soc.* **2009**, *131*, 9813.

(9) (a) Abrahamsson, M.; Lundqvist, M. J.; Wolpher, H.; Johansson, O.; Eriksson, L.; Bergquist, J.; Rasmussen, T.; Becker, H.-C.; Hammarström, L.; Norrby, P.-O.; Åkermark, B.; Persson, P. *Inorg. Chem.* **2008**, *47*, 3540. (b) Österman, T.; Abrahamsson, M.; Becker, H.-C.; Hammarström, L.; Persson, P. *J. Phys. Chem. A* **2012**, *116*, 1041. (c) Alary, F.; Boggio-Pasqua, M.; Heully, J.-L.; Marsden, C. J.; Vicendo, P. *Inorg. Chem.* **2008**, *47*, 5259. (d) Heully, J.-L.; Alary, F.; Boggio-Pasqua, M. *J. Chem. Phys.* **2009**, *131*, 184308. (e) Yang, L.; Okuda, F.; Kobayashi, K.; Nozaki, K.; Tanabe, Y.; Ishii, Y.; Haga, M.-a. *Inorg. Chem.* **2008**, *47*, 7154. (f) Österman, T.; Persson, P. *Chem. Phys.* **2012**, *407*, 76.

(10) Frisch, M. J.; et al. *Gaussian 09*, revision C.1; Gaussian, Inc.: Wallingford, CT, 2010.

(11) (a) Perdew, J. P.; Burke, K.; Ernzerhof, M. *Phys. Rev. Lett.* **1996**, *77*, 3865. (b) Perdew, J. P.; Burke, K.; Ernzerhof, M. *Phys. Rev. Lett.* **1997**, *78*, 1396. (c) Adamo, C.; Barone, V. *J. Chem. Phys.* **1999**, *110*, 6158.

(12) (a) Barone, V.; Cossi, M. *J. Phys. Chem. A* **1998**, *102*, 1995. (b) Cossi, M.; Rega, N.; Scalmani, G.; Barone, V. *J. Comput. Chem.* **2003**, *24*, 669.

(13) (a) Fukui, K. *Acc. Chem. Res.* **1981**, *14*, 363. (b) Hratchian, H. P.; Schlegel, H. B. In *Theory and Applications of Computational Chemistry: The First Forty Years*; Dykstra, C. E.; Frenking, G.; Kim, K. S.; Scuseria, G. E., Eds.; Elsevier: Amsterdam, 2005; pp 195−249.

(14) (a) Harvey, J. N.; Aschi, M. *Phys. Chem. Chem. Phys.* **1999**, *1*, 5555. (b) Harvey, J. N.; Aschi, M.; Schwarz, H.; Koch, W. *Theor. Chem. Acc.* **1998**, *99*, 95.

(15) (a) Stratmann, R. E.; Scuseria, G. E.; Frisch, M. J. *J. Chem. Phys.* **1998**, *109*, 8218. (b) Bauernschmitt, R.; Ahlrichs, R. *Chem. Phys. Lett.* **1996**, *256*, 454. (c) Casida, M. E.; Jamorski, C.; Casida, K. C.; Salahub, D. R. *J. Chem. Phys.* **1998**, *108*, 4439.

(16) Andrae, D.; Häussermann, U.; Dolg, M.; Stoll, H.; Preuss, H. *Theor. Chim. Acta* **1990**, *77*, 123.

(17) Ehlers, A. W.; Böhme, M.; Dapprich, S.; Gobbi, A.; Höllwarth, A.; Jonas, V.; Köhler, K. F.; Stegmann, R.; Veldkamp, A.; Frenking, G. *Chem. Phys. Lett.* **1993**, *208*, 111.

(18) (a) Hehre, W. J.; Ditchfield, R.; Pople, J. A. *J. Chem. Phys.* **1972**, *56*, 2257. (b) Hariharan, P. C.; Pople, J. A. *Theor. Chim. Acta* **1973**, *28*, 213. (c) Francl, M. M.; Pietro, W. J.; Hehre, W. J.; Binkley, J. S.; Gordon, M. S.; Defrees, D. J.; Pople, J. A. *J. Chem. Phys.* **1982**, *77*, 3654.

(19) Glendening, E. D.; Reed, A. E.; Carpenter, J. E.; Weinhold, F. *NBO*, version 3.1; University of Wisconsin: Madison, 1996.

(20) Tenderholt, A. L. *QMForge*, version 2.1; Stanford University: Stanford, CA, 2007.

(21) Kasha, M. *Discuss. Faraday Soc.* **1950**, *9*, 14.

(22) Fraga, S.; Karwowski, J.; Saxena, K. M. S. *Handbook of Atomic Data*; Elsevier Scientific: Amsterdam, 1976.

(23) Sotoyama, W.; Satoh, T.; Sato, H.; Matsuura, A.; Sawatari, N. J. *Phys. Chem. A* **2005**, *109*, 9760.